Rosetta Alice/VIRTIS observations of the water vapour UV electroglow emissions around comet 67P/Churyumov-Gerasimenko

Jean-Yves Chaufray, Dominique Bockelée-Morvan, Jean-Loup Bertaux, Stéphane Erard, Paul D. Feldman, Fabrizio Capaccioni, Eric Schindhelm, Cédric Leyrat, Joel Wm. Parker, Gianrico Filacchione, et al.

Monthly Notices
of the
ROYAL ASTRONOMICAL SOCIETY

MNRAS **469,** S416–S426 (2017)
Advance Access publication 2017 July 27

doi:10.1093/mnras/stx1895

Rosetta Alice/VIRTIS observations of the water vapour UV electroglow emissions around comet 67P/Churyumov–Gerasimenko

J.-Y. Chaufray,[1★] D. Bockelée-Morvan,[2] J.-L. Bertaux,[1] S. Erard,[2] P. D. Feldman,[3] F. Capaccioni,[4] E. Schindhelm,[5] C. Leyrat,[2] J. Parker,[5] G. Filacchione,[4] M. F. A'Hearn,[6] L. M. Feaga,[6] J. Noonan,[5] B. Keeney,[5] A. J. Steffl,[5] S. A. Stern,[5] H. A. Weaver,[7] T. Broiles,[8†] J. Burch,[8] G. Clark[7] and M. Samara[9]

[1]*LATMOS/IPSL, UPMC Univ. Paris 06 Sorbonne Universités, UVSQ, CNRS, 75252 Paris Cedex 05, France*
[2]*LESIA, Observatoire de Paris, LESIA/CNRS, UPMC, Université Paris Diderot, F-92195 Meudon, France*
[3]*Department of Physics and Astronomy, Johns Hopkins University, Baltimore, MD 21218, USA*
[4]*INAF-IAPS, Istituto di Astrofisica e Planetologia Spaziali, via del fosso del Cavaliere 100, I-00133 Rome, Italy*
[5]*Department of Space Studies, Southwest Research Institute, Boulder, CO 80302, USA*
[6]*Department of Astronomy, University of Maryland, College Park, MD 20742, USA*
[7]*Applied Physics Laboratory, Johns Hopkins University, MD 20723, USA*
[8]*Space Science and Engineering Division, Southwest Research Institute, San Antonio, TX 78238, USA*
[9]*Heliophysics Division, Goddard Space Flight Center, Greenbelt, MD 20771, USA*

Accepted 2017 July 24. Received 2017 July 17; in original form 2017 April 12

ABSTRACT

Several UV emission lines of the coma of 67P/Churyumov–Gerasimenko have been observed by Alice/*Rosetta* before the 67P/CG perihelion. The H and O emissions are mainly produced by impact dissociation of water molecules by suprathermal electrons. In this paper, we explore further the electron dissociative excitation of H_2O to produce the UV emissions by using simultaneous observations of water and H Lyman β done by the VIRTIS-H and Alice instruments during four periods of time in 2014 December, 2015 March and 2015 May. We used simple theoretical considerations to link the UV brightness to the water vapour column density. Two cases are studied. In the first case, we assume the suprathermal electron density is decreasing radially as the thermal electron population; in the second case, we assume the suprathermal electron density does not vary radially. The second case seems more consistent with the Rosetta Plasma Consortium Ion and Electron Sensor measurements during 2015 March and May. The efficiency of the electron dissociative excitation of H_2O is lower during the three last periods of time studied compared to the first period in 2014 December. The variability of the efficiency of the electron dissociative excitation between the four studied periods is not simply inversely proportional to the square of the comet–Sun distance but is most likely associated with the variability of the suprathermal electron distribution.

Key words: radiation mechanisms: non-thermal – comets: individual: 67P/CG.

1 INTRODUCTION

Rosetta insertion in-orbit around the nucleus of comet 67P/Churyumov–Gerasimenko has allowed *in situ* and remote sensing observations of both the nucleus and the coma with unprecedented spatial resolution. As a result, some new aspects of cometary physics have been discovered. One such discovery is in the UV wavelengths observed by the Alice spectrograph on board *Rosetta* (Feldman et al. 2015). The emissions of atomic lines of H, O and C were anticipated because they had been measured by several observatories, i.e. International Ultraviolet Explorer, the *Hubble Space Telescope* (Lupu et al. 2007; Weaver et al. 2011) and the Far Ultraviolet Spectroscopic Explorer (Feldman, Weaver & Burgh 2002; Weaver et al. 2002). These atomic emissions are due to resonance scattering of solar photons on atoms produced from the photolysis of H_2O and CO_2, allowing us to derive production rates of both these mother molecules. The most conspicuous spectral features measured by Alice spectrograph were, as expected, the H lines

★ E-mail: chaufray@latmos.ipsl.fr
† Present address: Space Science Institute, Boulder, CO 80301, USA.

at Ly α (121.6 nm), Ly β (102.5 nm) and O I at 130.4 nm (Feldman et al. 2015). However, sometimes during the escort phase, the absolute intensities of the atomic lines were much different from expected resonance scattering calculations performed for the H_2O production rate as determined from other instruments on board *Rosetta*. For instance, the Lyman β intensity was sometimes more than one order of magnitude larger than expected (Feldman et al. 2015). In addition, some line ratios were inconsistent with the H_2O solar photolysis model. For instance, the O I 135.6 nm was unexpectedly bright with respect to the O I at 130.4 nm (Feldman et al. 2015). The O I 135.6 nm line is a forbidden line and therefore if the resonant scattering is the main source of emission its brightness should be much weaker than the O I 130.4 nm.

The explanation of this unexpectedly bright emission at 135.6 nm with respect to the O I 130.4 nm emission was that Alice was the first UV spectrograph to resolve scales within 1 km from the nucleus, where H_2O dominates with respect to its photodissociation products (H, O, OH) in the coma, and what was seen was rather the result of a newly observed comet phenomenon, the electron dissociative excitation of water molecules (Feldman et al. 2015). The electrons are dissociating the H_2O molecule, and if their energy is sufficient, the O and H atoms are produced in an excited state, which de-excite spontaneously with what could be called an electroglow emission of the lines specific to the atom (the Lyman series for H, several lines for O, including O I 130.4 nm and O I 135.6 nm). In general, solar wind electrons have a mean energy of 5 eV, too small to produce H_2O dissociative excitation. Rather, the source of exciting electrons is photoionization of H_2O, and the resultant photoelectrons have peak energies in the range of 0–70 eV (Körösmezey et al. 1987). These energetic electrons have been detected by the Rosetta Plasma Consortium Ion and Electron Sensor (RPC-IES) instrument on *Rosetta* (Clark et al. 2015), although the measurement refers to a flux measured at the spacecraft, not near the surface of the comet as observed by Alice.

Before its perihelion, the atmosphere of comet 67P/Churyumov–Gerasimenko (67P/CG) was mainly composed of H_2O and CO_2 ejected from the nucleus (Bockelée-Morvan et al. 2015; Feldman et al. 2015; Le Roy et al. 2015). The gas ejection from the nucleus was not uniform (Luspay-Kuti et al. 2015), and controlled by the solar illumination (Bieler et al. 2015). The neck region was the most productive in water vapour (Bockelée-Morvan et al. 2015; Lee et al. 2015), while CO_2 ejection was mostly in the Southern hemisphere (Hassig et al. 2015; Migliorini et al. 2016). This non-uniformity of the nucleus outgassing led to a highly heterogeneous coma near the nucleus (Bieler et al. 2015; Fougere et al. 2016a,b). This coma is partially ionized forming a plasma of cometary origin close to the nucleus (Edberg et al. 2015; Odelstad et al. 2015). This cometary plasma can interact with the solar wind. This interaction is strongly dependent on the outgassing rate (Szego et al. 2000). The newborn water ions can be accelerated by the solar wind motional electric field (Nilsson et al. 2015). These pick-up ions generate waves that transfer part of the solar wind energy to the cometary plasma (e.g. Coates 2004). The detection of accelerated water ions in the environment of 67P/CG as well as the deflection of the solar wind indicate that the pick-up ions process is effective at 67P/CG (Nilsson et al. 2015).

Several populations of electrons are observed in the cometary plasma environment: A 'cold' population of cometary origin (few electronvolts) not directly measured by RPC-IES due to their low energy (Odelstad et al. 2015; Broiles et al. 2016), a 'warm' population (between ∼10 and 100 eV) probably of cometary origin and a 'hot' population (>100 eV) from the solar wind halo (Zwinckl et al. 1986; Clark et al. 2015; Broiles et al. 2016). The origin of the 'warm' electron population observed in the plasma environment of 67P/CG is not fully understood. The electric field associated with the waves generated by the H_2O^+ pick-up ions could accelerate the newborn photoelectrons to several hundreds of electronvolts as observed by RPC-IES (Clark et al. 2015) and produce this 'warm' population. Clark et al. (2015) show the dynamics of these acceleration processes leading to large temporal/spatial variations of the electron energy flux distribution from 2014 August to December. The presence of a large amount of suprathermal electrons (the 'warm' population) in the plasma environment of 67P/CG is responsible of the UV emission lines observed by Alice (Feldman et al. 2015). These authors show that the relative line intensities of the H I and O I emissions were consistent with the expected ratios from electron impact (at ∼100 and ∼200 eV) on water vapour.

In this paper, we use simultaneous observations of water and H Lyman β done by the VIRTIS-H and Alice instruments, respectively, to estimate the efficiency of this mechanism at different periods before the perihelion of 67P/CG. Alice and VIRTIS-H are boresight mounted on *Rosetta*, and a number of measurements have been acquired simultaneously by the two instruments along the same line of sight (LOS). The idea of this study is to explore further the electron dissociative excitation of H_2O to produce the UV emissions. Knowing the excitation cross-sections for the UV lines (Makarov et al. 2004; Itikawa and Mason, 2005), the H_2O column densities and with a model of electron distribution based on RPC-IES data, it is hoped to find a consistent quantitative description of this new comet phenomenon. In some sense, the coma is used as a laboratory, where several instruments can monitor the experimental conditions for an accurate description of the involved mechanisms of UV emission. In the next section, we will describe the observations done by VIRTIS-H and Alice during the four campaigns studied in this paper. A simple theoretical approach is described in Section 3 to study the dependence of the brightness with the water column density. This relation is then compared to the observations in Section 4 and followed by a conclusion.

2 OBSERVATIONS

2.1 VIRTIS observations

The Visible InfraRed Thermal Imaging Spectrometer (VIRTIS) (Coradini et al. 2007) is composed of two channels: VIRTIS-M, a visible-infrared imaging spectrometer operating both in the visible and the IR (0.25–5 μm) with a spectral resolution of $\lambda/\Delta\lambda \sim 70$–300, and VIRTIS-H, a single aperture infrared spectrometer (1.9–5 μm) with a higher spectral resolution $\lambda/\Delta\lambda \sim 1300$–3000. The instantaneous field of view of the VIRTIS-H instrument is 0.58×1.74 mrad^2. Vibrational bands of CO_2 and H_2O have been detected in the coma of 67P/Churyumov–Gerasimenko since 2014 October as reported by Bockelée-Morvan et al. (2015), Migliorini et al. (2016) and Fink et al. (2016). The ro-vibrational structure of the H_2O bands at 2.67 μm is partly resolved by VIRTIS-H. These emission bands result from the fluorescence excitation by solar infrared radiation (Bockelée-Morvan and Crovisier 1987, Crovisier 1987, Bockelée-Morvan et al. 2004). In optically thin conditions, the water column density along the LOS can be derived straightforwardly from the band intensity, using a g factor $g_f = 3.349 \times 10^{-4}$ s^{-1} at 1 au (excitation rate of one H_2O molecule, Villanueva et al. 2012). The water column densities derived by VIRTIS-H from 2014 November to 2015 January at distances from 67P/CG surface of typically 2–3 km were found to vary between $\sim 4 \times 10^{18}$ m^{-2} and 1.1×10^{20} m^{-2}

Table 1. Selected set of observations acquired by VIRTIS-H and the associated Alice observations. Some geometric parameters of the observations are also given in columns 3 and 4. The impact parameter is the distance between the line of sight and the comet centre. All times are given in Universal Time.

VIRTIS-H Obs Id	Time of the VIRTIS cube acquisition.	Comet–Sun distance (au)	Impact parameter/spacecraft distance above cometary centre	Number of VIRTIS subfiles	Number of Alice files associated, and temporal range including these files
003 762 11338	03/12/14 (07:01 → 08:52)	2.85	∼2 km/30 km	1	11 (07:02 → 08:49)
003 763 02843	04/12/14 (08:26 → 10:17)	2.84	∼1.5 km/25 km	1	10 (08:36 → 10:07)
003 764 66638	06/12/14 (05:57 → 06:47)	2.83	∼2.5 km/20 km	1	4 (06:05 → 06:38)
003 764 70838	06/12/14 (07:06 → 07:57)	2.83	∼2 km/20 km	1	5 (07:10 → 07:53)
003 767 06343	09/12/14 (00:31 → 02:22)	2.81	∼3 km/20 km	1	8 (01:00 → 02:15)
003 767 69292	09/12/14 (18:02 → 19:56)	2.80	∼2 km/20 km	1	11 (18:05 → 19:53)
003 847 45481	12/03/15 (01:13 → 05:36)	2.12	∼3 km/80 km	16	22 (01:39 → 05:47)
003 847 65982	12/03/15 (07:12 → 11:01)	2.12	∼3 km/80 km	16	14 (07:51 → 10:54)
003 847 82294	12/03/15 (11:44–12:12)	2.12	∼3 km/80 km	16	1 (12:04)
003 848 30143	13/03/15 (01:01 → 02:17)	2.12	∼5 km/80 km	16	2 (01:12 → 02:04)
003 848 41114	13/03/15 (04:04 → 07:23)	2.12	∼5 km/80 km	16	11 (04:07 → 06:49)
003 901 52259	13/05/15 (15:30 → 19:33)	1.64	∼8 km/160 km	16	19 (15:36 → 19:28)
003 901 73045	13/05/15 (21:30 → 00:39)	1.64	∼8 km/160 km	16	15 (21:37 → 00:36)
003 911 89569	25/05/15 (15:42 → 19:32)	1.56	∼13 km/240 km	16	16 (15:50→ 19:20)
003 912 09562	25/05/15 (21:16 → 00:25)	1.56	∼13 km/250 km	16	14 (21:37 → 00:16)
003 912 95114	26/05/15 (21:02 → 00:02)	1.56	∼16 km/300 km	16	12 (21:10 → 23:59)

when the comet–Sun distance was 2.91–2.47 au (Bockelée-Morvan et al. 2015). The VIRTIS-H calibrated data are referred as to cubes because they are three dimensional: intensity versus wavelength and acquisition number. In this paper, we used limb observations of the coma performed by VIRTIS-H in 2015 March and May, in addition to published measurements in 2014 December (Table 1). The derivation of the water column density was performed using the same method as presented by Bockelée-Morvan et al. (2015).

Four periods of observations of the water column density were considered. The first period is 2014 December 3–9 (Bockelée-Morvan et al. 2015). However, the two cubes obtained on 2014 December 8 are not included because no Alice observations are available after 12:00 UT. One of the largest water vapour column density of the full set of observations studied by Bockelée-Morvan et al. 2015 was observed during this period, on 2014 December 4. The second period is 2015 March 12–13 and is composed of five cubes with a total of 3456 acquisitions (individual spectra). The third period (2015 May 13) is composed of two cubes for a total of 3520 acquisitions and the last period (2015 May 25–26) is composed of three cubes for a total of 8512 acquisitions. It may be noted that we have avoided the six periods studied with Alice for outburst conditions linked to O_2 outgassing (Feldman et al., 2016) but a smaller outburst occurred on May 13.

2.2 Alice observations

The UV spectrometer Alice has been designed to study the *in situ* far-ultraviolet (70–205 nm) spectrum of comet 67P/Churyumov–Gerasimenko. It is a lightweight, low-power, imaging spectrograph consisting of a single parabolic off-axis mirror, a slit and a concave holographic grating dispersing the UV spectrum of each point of the slit along one dimension of a 2D photon counting detector, in a direction perpendicular to the slit. The slit is in the shape of a dog bone, 5.5° long, with a width of 0.05° in the central 2.0°, while the ends are 0.10° wide, giving a spectral resolution between 8 and 12 Å for extended sources that fill its field of view. Each spatial pixel or row along the slit is 0.30° long. A row of the detector corresponds to the spectrum of a given part of the slit. Accumulating the counted photons for some time produces a spectrum for each spatial row, allowing both spectral studies and spatial variations of the emissions. The spectral range covers the atomic hydrogen Lyman α and Lyman β lines, and several atomic oxygen lines

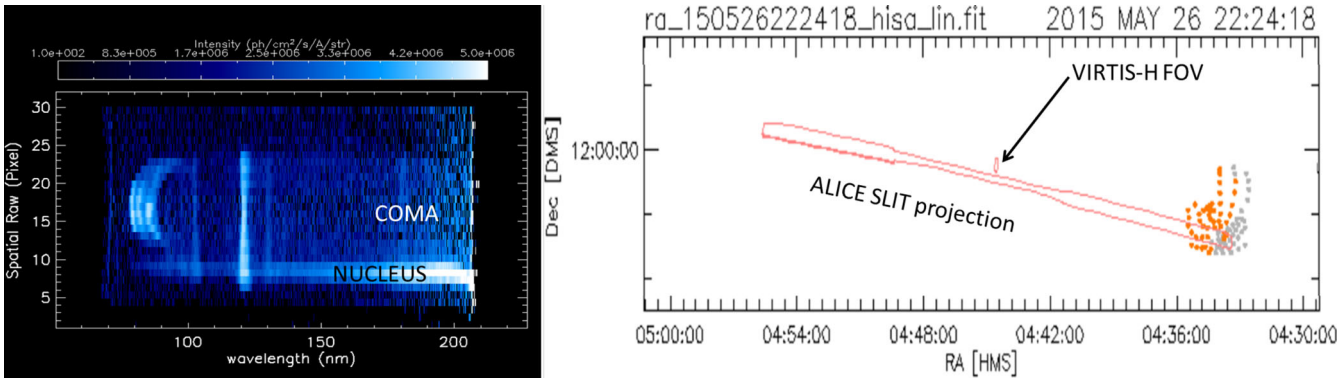

Figure 1. Left: Image of the detector of Alice observed during one observation on 2015 May 26. Right: The geometry of the observation and the sky projection of the Alice slit and VIRTIS field of view are indicated in red. The small VIRTIS field of view is indicated by the arrow. The right figure is derived from geoviz tool using the SPICE digital Shape Kernel (DSK) for the comet. Orange dots indicate the sunlit face of the comet and the grey dot the unlit portion of the comet.

(Stern et al. 2007, Feldman et al. 2015). Details of the instrument have been given by Stern et al. (2007).

The image histogram mode, the primary mode used by Alice, is described in Stern et al. (2007). In this mode, the acquisition memory is used as a two-dimensional array with a size corresponding to the spectral and spatial dimensions of the detector array (1024 × 32). An example of histogram obtained on 2015 May 26 is displayed in Fig. 1 (left) associated with the geometry of the observation (right) during this period.

The shape of the slit can be seen easily from the strong Lyman α emission line. An odd–even effect from row to row is also visible on the Lyman α line. The 'odd–even' effect is not a sensitivity effect, but due to the microchannel plate electronics not correctly calculating the Y-position (spatial location) of photon events, so that some fraction of the events are placed in a row adjacent to where they actually hit the detector. This odd–even effect can lead to ∼15 per cent variations in the Lyman β brightness. The nucleus of 67P/CG is observed on the spatial rows 7, 8 and 9 as expected from the geometry (Fig. 1, right). The coma, including the associated atomic hydrogen (H 102.5, and 121.6 nm) and oxygen emission lines (130.4 nm and the less intense O 135.6 nm) produced from water vapour electron dissociative excitation, are observed on the spatial rows 10–24. The H 121.6 nm is dominated by the interplanetary emission (few hundreds of Rayleigh) and not used in this study. The coma emissions lines have been presented and discussed by Feldman et al. (2015). The structure observed between 75 and 95 nm called the 'chameleon' is presumably associated with dust entering the spectrometer (see Noonan et al. 2016 for more details). On the right part of Fig. 1, the field of view of both Alice (slit projection) and VIRTIS-H (small rectangle near the black arrow) are indicated.

For this study, we use several 10 min spectro-image histograms during which the coma of 67P was observed. We choose only observations starting, and during more than 3 min, in the time of a subcube acquisition by VIRTIS in order to have simultaneous observations for all VIRTIS cube acquisition. This length is a balance to have the best temporal coverage between the subcube acquisition and the Alice histograms keeping at least one Alice histogram for each VIRTIS cube acquisition. We have checked that changing 3 min to 1 or 5 min does not change the results presented below but just degrade the simultaneous coverage (1 min) or decrease the number of Alice histograms per VIRTIS cube (5 min). If we choose 5 min, no Alice histograms could be found for the VIRTIS cube 003 847 82294 and 003 848 30143. For the three last campaigns, the VIRTIS cube acquisition has been split into 16 subcubes each one associated with 0, 1 or 2 histograms of Alice when using our 3 min criteria. The time intervals covered by the Alice and VIRTIS-H data during for each subcube acquisition periods studied here are never exactly the same and possible effects of this difference will be discussed.

The data selected for this study are indicated in the last column of Table 1. The projection of the Alice and VIRTIS-H fields of view on the sky for the 2015 March 12–13 and 2015 May 13 period are displayed in Fig. 2. For all the data analysed here, we only use the UV brightness derived along the spatial row 15 (middle of the slit) of Alice, close to the VIRTIS-H field of view at a few kilometres above the surface. The odd–even effect can lead to 15 per cent variations from one row to another. Such variation is small given the simple theory used and will not affect our conclusions.

3 THEORETICAL CONSIDERATIONS

Before studying the correlation between the water vapour column density measured by VIRTIS and the Lyman β brightness measured by Alice, we present the expected relation between these two parameters from simple theoretical considerations.

3.1 Water vapour column density

We consider a Haser distribution for the water vapour and neglect the exponential decrease related to water photodissociation.

$$n_{\mathrm{H_2O}}(r) = \frac{Q}{4\pi u_{\mathrm{n}}}\frac{1}{r^2}, \tag{1}$$

where Q is the water sublimation rate and u_{n} the neutral velocity.

Assuming that the spacecraft distance is much larger than the impact parameter (p), the water vapour column density integrated along the VIRTIS LOS is given by

$$N_{\mathrm{H_2O}} = \int_0^\infty n_{\mathrm{H_2O}}(s)\,\mathrm{d}s = \frac{Q}{4u_{\mathrm{n}}}\frac{1}{p}, \tag{2}$$

where s is the distance along the LOS from the spacecraft ($s = 0$ at the spacecraft position), $r^2 = p^2 + (s - S_{\mathrm{sc}})^2$, where S_{sc} is the distance between the spacecraft and the tangent point of the LOS. As shown in Table 1, the spacecraft cometocentric distance is about 10 times larger than the impact parameter. Taking into account the cometocentric distance of the spacecraft will reduce the water

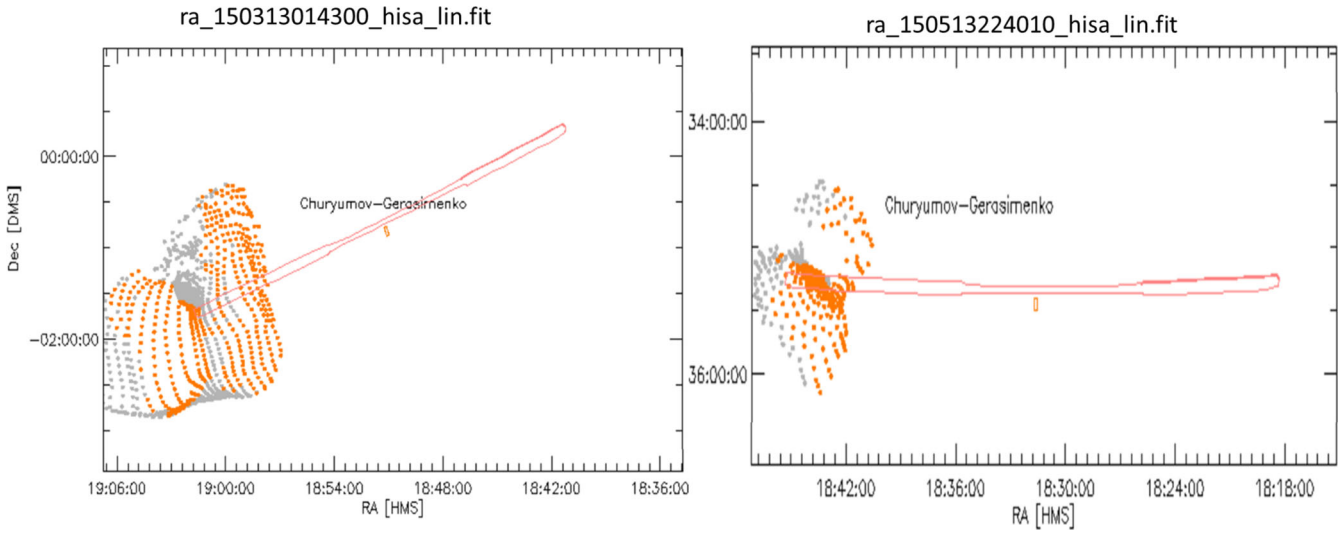

Figure 2. Geometry of the observation and the sky projection of the Alice slit and VIRTIS field of view for the observations on 2015 March 13 (left) and 2015 May 13 (right). The figure is derived from geoviz tool using the SPICE digital Shape Kernel (DSK) for the comet. Orange dots indicate the sunlit face of the comet and the grey dot the unlit portion of the comet.

column given by equation (2):

$$\frac{N(\infty)-N(S_{sc})}{N(\infty)} = 1-\left[\frac{1}{2}+\frac{1}{\pi}\arctan\left(\frac{S_{sc}}{p}\right)\right] = \left[\frac{1}{2}-\frac{1}{\pi}\arctan\left(\frac{S_{sc}}{p}\right)\right]. \quad (3)$$

For $S_{sc}/p = 10$, we find an error of ∼3 per cent. This difference will be neglected in this study.

3.2 Electron density

We assume that the medium is collisionless and solve the continuity equation for electrons neglecting the chemical loss term and using a uniform electron velocity. The coma is assumed to be primarily composed of water, the ionization by energetic electron is ignored as done by Madanian et al. (2016), though these assumptions are not always correct (e.g. Galand et al. 2016).

The typical observed water vapour slant density is $\sim 10^{20}$ m^{-2}. The absorption cross-section for H_2O can reach 2×10^{-21} m^2 between 5 and 98 nm (Schunk and Nagy 2009). Therefore, the coma can be considered as optically thin. In this case, considering a spherical shell of thickness dr at distance r from the nucleus (also valid for a radial expansion within a cone), the continuity equation for electrons can be written:

$$\frac{\partial n_e}{\partial t}+\frac{1}{r^2}\frac{\partial (n_e u_e r^2)}{\partial r} = \nu n_{H_2O}(r). \quad (4)$$

At steady state, the general solution, assuming that the ionospheric density is 0 at the cometary surface r_s is given by (Galand et al. 2016)

$$n_e(r) = \frac{\nu Q}{4\pi u_e u_n}\frac{(r-r_s)}{r^2}, \quad (5)$$

where we have used a Haser distribution for the local density of water vapour (equation 1). ν is the ionization frequency of H_2O molecules, Q is the water sublimation rate, u_n and u_e are the neutral and electron radial velocities, respectively, and r is the distance to the comet centre. We have neglected the photoelectrons emitted from the nucleus (Nordheim et al. 2015). According to Edberg et al. (2015), the observed electron density radial variation can be described by a $1/r$ radial profile at a few kilometres above the nucleus so we will neglect the term in r_s/r^2 in the following.

The electron density is therefore given by

$$n_e(r) = \frac{\nu Q}{4\pi u_e u_n}\frac{1}{r}. \quad (6)$$

In the following, we will use $u_e = 0.7$ km s^{-1} based on the ion velocity from Galand et al (2016). This value could slightly vary with r due to the motional electric field (Galand et al. 2016). Such variation is not considered in this paper. If we assume that the density of energetic electrons (energy between 10 and 300 eV necessary for electron dissociative excitation of H_2O) n_{es} is proportional to the electron density (case 1):

$$n_{es}(r) = \alpha\frac{\nu Q}{4\pi u_e u_n}\frac{1}{r}. \quad (7a)$$

Then the suprathermal electron density should vary as $1/r$. The recent study by Madanian et al. (2016) seems to indicate very few variations of the suprathermal electron density with radial distance from 20 to 250 km (case 2) suggesting that α increases linearly with r and

$$n_{es}(r) = n_{es,0}. \quad (7b)$$

In the following, we will study both cases called case 1 (equation 7a) and case 2 (equation 7b).

3.3 Lyman β brightness

We estimate the contribution of resonant scattering of the solar photons by cometary H atoms (produced from H_2O photodissociation) and interplanetary hydrogen, using Alice data where the pointing is offset from the nucleus (2015 May 28, 20:11:17), at ∼150 km from the comet centre. The measured brightness of this background is ∼2–3 R. This value should change only slightly with the impact

parameter. The emission brightness for the H Lyman β line from electron dissociative excitation of H_2O is given by

$$I = \int_0^\infty g(T_e) n_{e,s}(s) n_{H_2O}(s) \mathrm{d}s, \tag{8}$$

where s is the distance from the spacecraft along the LOS, $g(T_e)$ is the electron dissociative excitation rate of the Lyman β line resulting from electron impact dissociation of H_2O as a function of the electron temperature (Feldman et al. 2015).

For case 1, using the expressions (7a) above for $n_{e,s}$ and equation (1) for n_{H_2O} as well as $r^3 = (p^2 + (s - s_{sc})^2)^{3/2}$, we find

$$I = \left(\frac{Q}{4\pi u_n}\right)\left(\frac{\alpha \nu Q}{4\pi u_n u_e}\right)\frac{g}{p^2} \times \left[\int_{-x_{sc}}^{0} \frac{1}{(1+x^2)^{3/2}}\mathrm{d}x + \int_0^\infty \frac{1}{(1+x^2)^{3/2}}\mathrm{d}x\right], \tag{9}$$

where $x = (s - S_{sc})/p$, and $x_{sc} = S_{sc}/pS_{sc}$ is the distance between the spacecraft and the tangent point of the LOS and p the impact parameter. This integral can be computed explicitly using

$$\int_0^{x_{sc}} \frac{1}{(1+x^2)^{3/2}}\mathrm{d}x = \left[\frac{x}{\sqrt{x^2+1}}\right]_0^{x_{sc}} = \frac{x_{sc}}{\sqrt{x_{sc,}{}^2+1}}$$

and when $x_{sc} = \infty$ it leads to

$$I = \frac{2\alpha\nu N_{H_2O}^2}{\pi^2 u_e} g(T_e) = k(T_e) N_{H_2O}^2. \tag{10a}$$

Assuming the spacecraft is far from the comet, equation (10a) leads to an error given by equation (11)

$$\frac{I(\infty) - I(S_{sc})}{I(\infty)} = 1 - \left[\frac{1}{2} + \frac{1}{2}\left(\frac{x_{sc}}{\sqrt{x_{sc}^2+1}}\right)\right] = \left[\frac{1}{2} - \frac{1}{2}\left(\frac{x_{sc}}{\sqrt{x_{sc}^2+1}}\right)\right] \tag{11}$$

lower than 1 per cent when the spacecraft cometocentric distance is 10 times the impact parameter.

For case 2, using the expression (7b), the brightness is given by the equation (10b)

$$I = n_{es0} N_{H_2O} g(T_e) = f(T_e) N_{H_2O}. \tag{10b}$$

The assumption of a spacecraft at infinity leads to no error in the second case.

If the suprathermal electron density decreased as the thermal electron density then the Lyman β brightness should vary as the square of the water column density and therefore as $\sim 1/p^2$, while it should vary as the water column density if the suprathermal electron density does not vary very much with cometocentric distance and therefore as $\sim 1/p$.

The Alice observations performed in May 25 and 26 encompass a cometocentric distance range from 5 to ~25 km (Fig. 2, right). The Lyman β brightness variations versus the impact parameter are displayed in Fig. 3 for the set of observations indicated in Table 1 during the 2015 May 25.

The variations of the Lyman β brightness could be reasonably reproduced with a $1/p^2$ profile or a $1/p$ profile. In the following, we will study both relations presented above between the Lyman β brightness measured by Alice and the water column density measured by VIRTIS at the same time. A decrease of the efficiency of the electron dissociative excitation process from 2014 December to 2015 March and May is found from both assumptions.

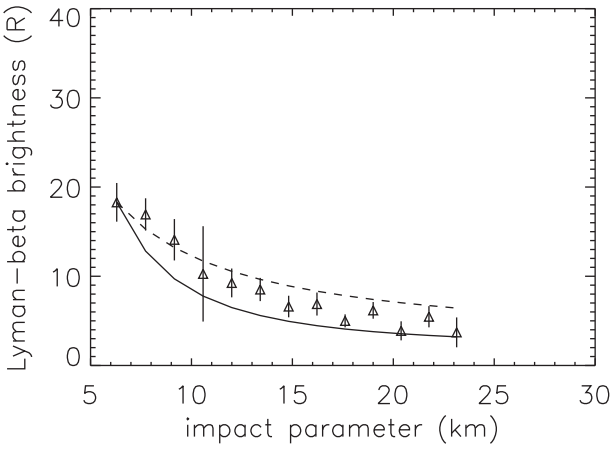

Figure 3. Variations of the Lyman β brightness (in Rayleigh) with the impact parameter derived from a set of observations in 2015 May 25 (triangles). The solid and dashed lines represent the profiles for $1/p^2$ and $1/p$ dependence, respectively, of the brightness plus 2 Rayleigh of background.

The factor k depends only on the ionization frequency ν, the electron radial velocity u_e, the proportion of suprathermal electron α and the g factor $g(T_e)$. Therefore, it should vary very slowly with the radial distance to the comet centre and should vary as ν ($\sim 1/d^2$) as a function of the Sun–comet distance d if the electron velocity and temperature are constant. Because of the simple approximation used in this approach, only an order of magnitude of this coefficient $k(T_e)$ will be considered. A more accurate approach solving the kinetic equations for the suprathermal electrons in the electromagnetic environment of the comet and taking into account non-spherical coma is beyond the scope of this paper.

The $g(T_e)$ factor can be estimated using the energy distribution of the energetic electron flux and the electron dissociative H Lyman β excitation cross-section from Makarov et al. (2004):

$$g\,(T_e) = \langle \sigma V \rangle = \frac{\int_E \sigma(E)\Phi(E)\mathrm{d}E}{n_{e,s}}, \tag{12}$$

with $n_{e,s}$ is the suprathermal electron density, and the integral computed from 17.5 to 600 eV.

$g(T_e)$ was estimated to 2×10^{-10} cm^3 s^{-1} by Feldman et al. (2015), assuming a Maxwellian distribution with $T_e = 25$ eV. Its variations with r (comet centre distance) and d (Sun distance) will be discussed in Section 5.

4 RESULTS

Using the four periods of observations, we may check if the simple theoretical relations given in the previous section are verified. The temporal variations of the water column density observed by VIRTIS-H and the brightness of the Lyman β emission of H are displayed in Fig. 4. The typical uncertainty on the derived Lyman β brightness (not shown in the figures) is 2 Rayleigh.

There is a correlation between the Lyman β brightness and the water vapour column density as expected for the mechanism producing the Lyman β brightness. An outburst of O_2, smaller than those reported by Feldman et al. (2016), was observed by Alice starting at UTC 21:37. As seen in Fig. 4(c), an increase of the H_2O column density and H Lyman β measured by VIRTIS-H and Alice is observed at the same time.

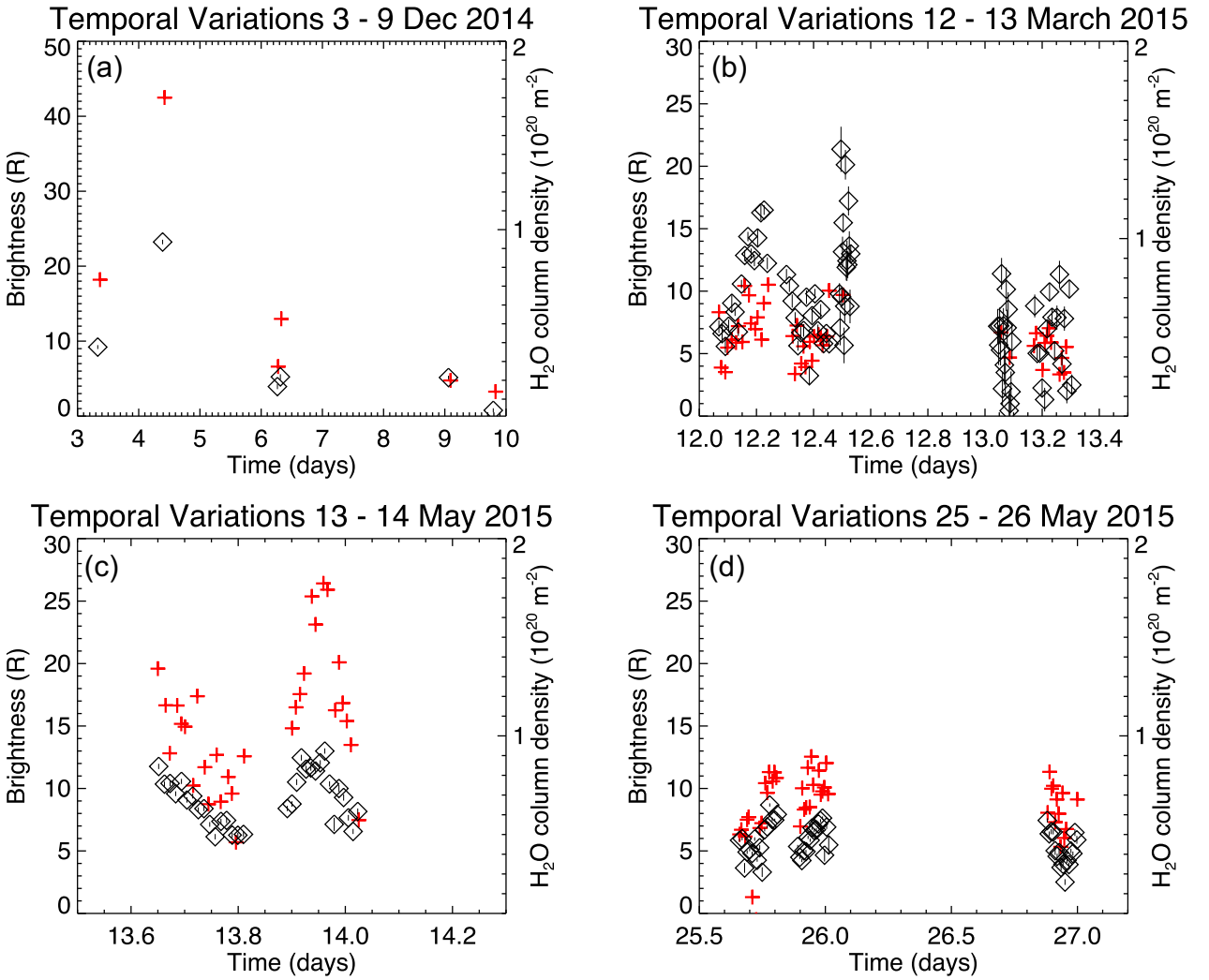

Figure 4. Temporal variations of the Lyman β brightness (red crosses) and water vapour column density (black diamonds) measured by Alice and VIRTIS, respectively, on 2014 December 3–9 (a), 2015 March 12 and 13 (b), 2015 May 13 and 14 (c) and 2015 May 25–26 (d). The error bars on the water vapour column density are indicated by the vertical black lines. The typical uncertainty on the derived Lyman β brightness is 2 Rayleigh.

From our simple theoretical considerations presented in Section 3, we have shown that the observed brightness should be proportional to the square of the water column density or to the water column density. The first case is studied in Section 4.1 and the second case in Section 4.2

4.1 Correlation between *I* and N^2

The Lyman β brightness versus the square of the water column density derived from the four campaigns is displayed in Fig. 5 as well as the best linear fit. For all the fits, we assume a 2 Rayleigh background as estimated from observations where the pointing was offset from the nucleus.

For the first campaign in 2014 December, the derived value of k is $\sim 4.9 \pm 0.2 \times 10^{-29}$ m^2 s^{-1}. The coefficient of linear correlation between the square of the water vapour column and the Lyman β brightness is 0.8. For the second campaign in 2015 March, the value of k is $\sim 7.2 \pm 0.7 \times 10^{-30}$ m^2 s^{-1}. The linear correlation between the square of the water vapour column and the Lyman β brightness is poor (coefficient $\sim$ 0.5). Several effects could lead to this poor correlation. First, the Lyman β brightness is low, between 5 and 10 Rayleigh, and the signal-to-noise ratio is not very good for these Alice observations. Secondly, large magnitude variations of the slant density are observed on very small time-scale during this campaign (e.g. near 12.5 March UT) and because the times of observation between VIRTIS-H and Alice does not match exactly it could lead to errors in the linear fit derivation. Contrary to other campaigns, the derived value of k is sensitive to the type of linear fit used. For example, if we impose a 0 value for the background, the coefficient k increases by 50 per cent, while for all other campaigns the coefficient varies by less than 30 per cent. For the third campaign done in May 2015, the value of k is $\sim 2.9 \pm 0.1 \times 10^{-29}$ m^2 s^{-1}. The linear correlation between the square of the water vapour column and the Lyman β brightness is good ($\sim$0.7). For the last campaign, the value of k is also $2.9 \pm 0.3 \times 10^{-29}$ m^2 s^{-1}. The correlation is rather reasonable ($\sim$0.6). The values of the parameter k derived for each set of observations are indicated in Table 2.

4.2 Correlation between *I* and *N*

The Lyman β brightness versus the water column density derived from the four campaigns is displayed in Fig. 6 as well as the best linear fit. For all the fits, we assume a 2 Rayleigh background as

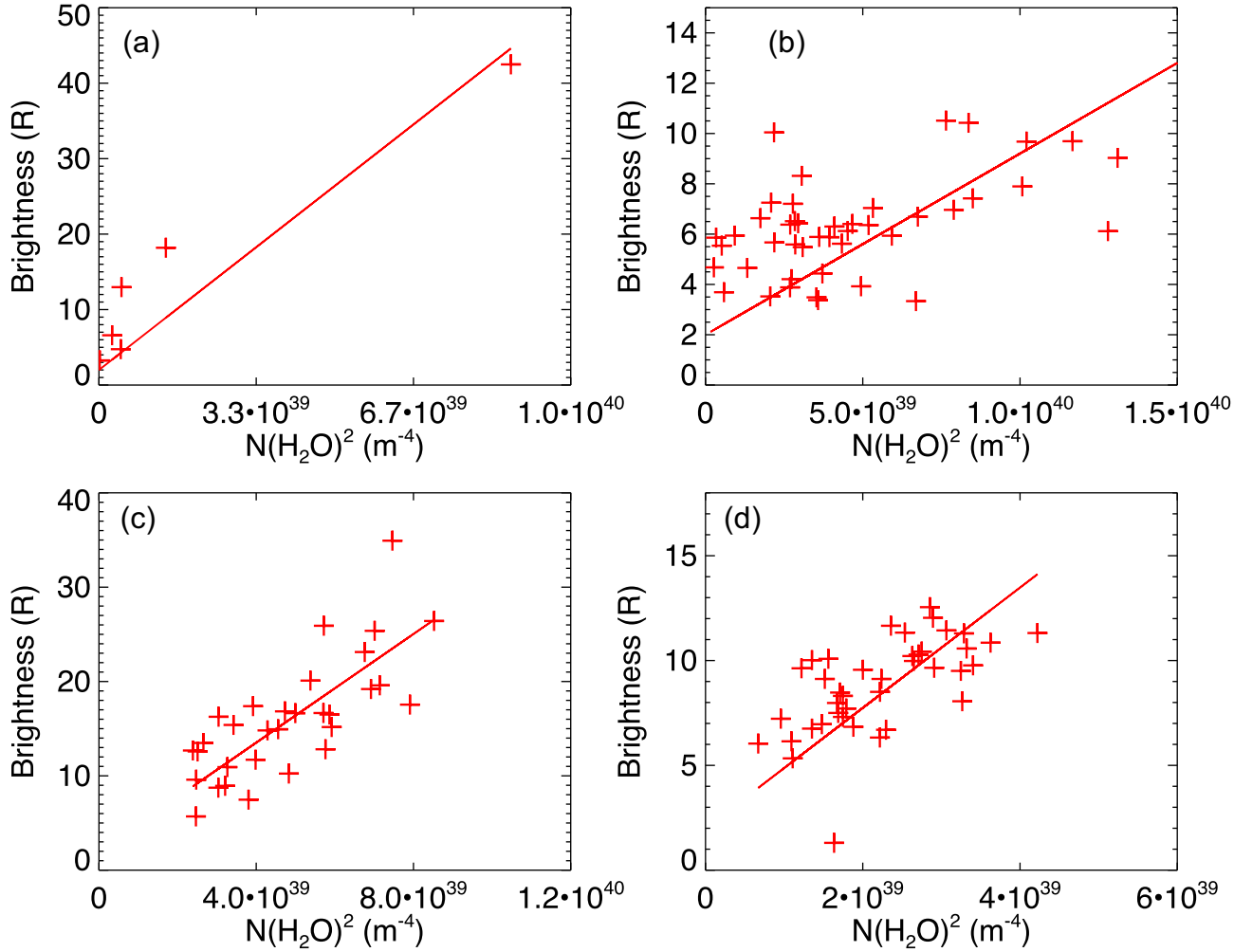

Figure 5. Lyman β brightness measured by Alice versus the square of the water vapour column density measured by VIRTIS-H on 2014 December 3–9 (a), 2015 March 12 and 13 (b), 2015 May 13 and 14 (c) and 2015 May 25–26 (d). The best linear fits are represented by the red lines.

Table 2. Parameters derived from the linear fit between the Lyman β brightness and the water column square for each period of observations. The theoretical value is also indicated.

Period of time	k parameter ($m^2\ s^{-1}$)	Linear correlation coefficient	k theoretical ($m^2\ s^{-1}$)
2014 December 4–9	$4.9 \pm 0.2 \times 10^{-29}$	0.80	1.3×10^{-28}
2015 March 12–13	$7.2 \pm 0.4 \times 10^{-30}$	0.51	2.4×10^{-28}
2015 May 13	$2.9 \pm 0.1 \times 10^{-29}$	0.73	4.0×10^{-28}
2015 May 25–26	$2.9 \pm 0.3 \times 10^{-29}$	0.59	4.4×10^{-28}

Table 3. Parameters derived from the linear fit between the Lyman β brightness and the water column for each period of observations.

Period of time	f parameter ($n_e \times g$) (s^{-1})	Linear correlation coefficient	$n_{e,s}$ (cm^{-3})
2014 December 4–9	$4.2 \pm 0.2 \times 10^{-9}$	0.82	52
2015 March 12–13	$6.3 \pm 0.3 \times 10^{-10}$	0.48	8
2015 May 13	$2.1 \pm 0.2 \times 10^{-9}$	0.72	28
2015 May 25–26	$1.5 \pm 0.1 \times 10^{-9}$	0.61	20

estimated from observations where the pointing was offset from the nucleus.

The derived values of f for the four campaigns of observation are $\sim 4.2 \pm 0.2 \times 10^{-9}\ s^{-1}$, $\sim 6.3 \pm 0.3 \times 10^{-10}$, $\sim 2.1 \times 10^{-9}$ and $\sim 1.5 \times 10^{-9}\ s^{-1}$, the derived values of f are given in Table 3. The linear correlation between the water vapour column and the Lyman β brightness is not different from the linear correlation between the Lyman β brightness and the square of the water vapour column, and it is not possible to discriminate the best relation from the correlation.

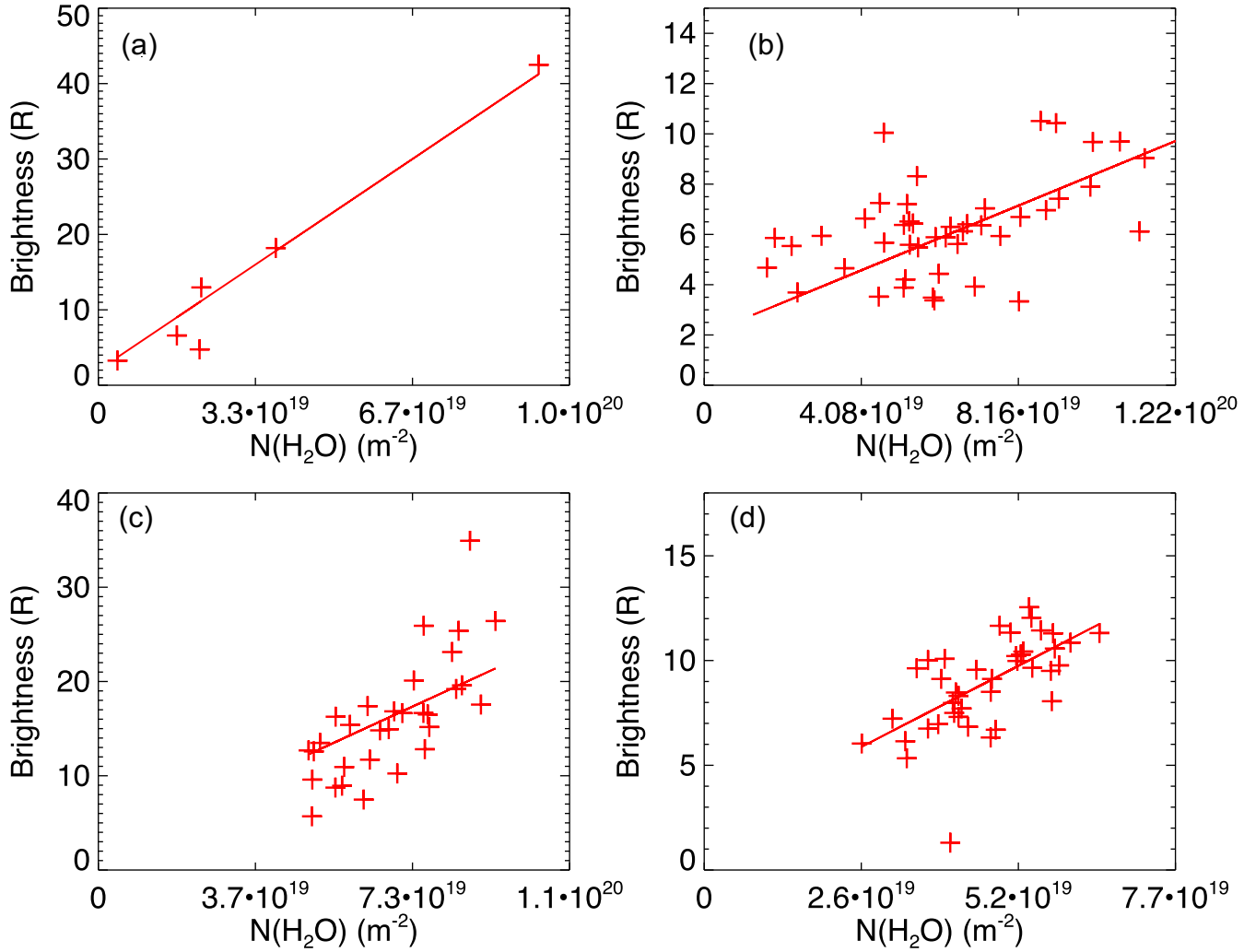

Figure 6. Lyman β brightness measured by Alice versus the water vapour column density measured by VIRTIS-H on 2014 December 3–9 (a), 2015 March 12 and 13 (b), 2015 May 13 and 14 (c) and 2015 May 25–26 (d). The best linear fits are represented by the red lines.

5 DISCUSSION

From equation (10a), we derive an analytical expression for the coefficient k. We can estimate its value from this equation and compare to the derived values from the observations. The water vapour photoionization rate at 1 au is between 3×10^{-7} and 8×10^{-7} s^{-1} (Huebner et al. 1992) and a value of about $\sim 7 \times 10^{-7}$ s^{-1} at 1 au was derived by Galand et al. (2016) for a coma composed of water vapour only. The cross-section dependence on electron energy for the production of a Lyman β photon is illustrated in Fig. 7. To derive it, we used the Lyman α excitation cross-section reduced by a factor 8 corresponding to the ratio of the Lyman α and Lyman β excitation cross-section for 200 eV electrons, the only value reported for Lyman β excitation cross-section (Makarov et al. 2004).

The emission rate $g(T_e)$ is estimated to 8×10^{-11} cm^3 s^{-1} for a Maxwellian distribution and an electron temperature T_e of 17 eV (Broiles et al. 2016).

We used $\alpha = 6.6 \times 10^{-2}$ corresponding to a mean suprathermal electron density of 20 cm^{-3} (Broiles et al. 2016) and a mean thermal electron density of 300 cm^{-3} (Edberg et al. 2015), this value is uncertain and will be discussed in the next section. For the observations performed in 2014 December, the theoretical value is slightly larger by about a factor 2.7 compared to the value derived from observations (Table 2), which is reasonable given the simple theory used in this paper. For the three other periods of observations, the theoretical values of k are 2.4×10^{-28}, 4.0×10^{-28} and

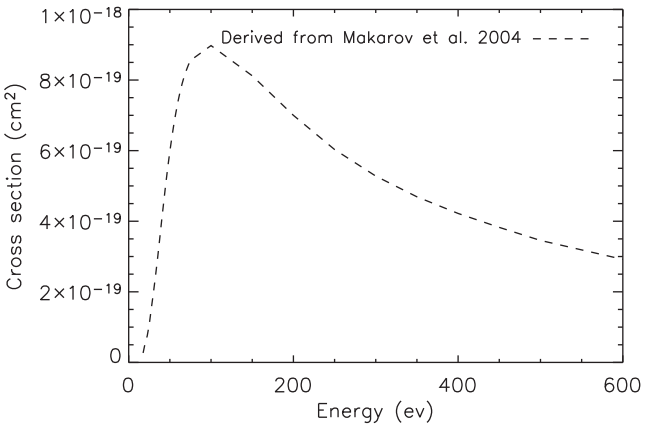

Figure 7. Cross-section for the emission of H Lyman β line at 102.5 nm for electron impact on H_2O.

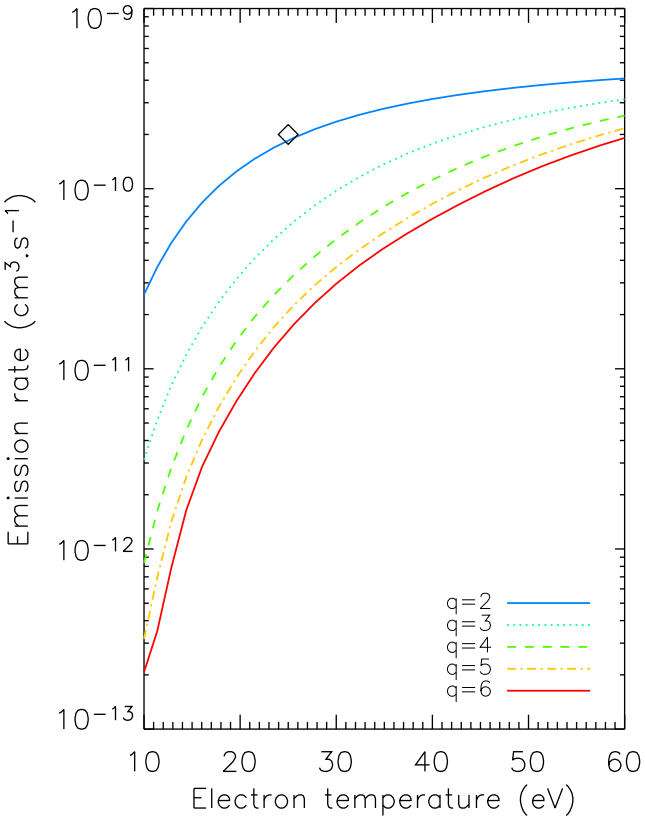

Figure 8. Estimated value of the emission rate $g(T_e)$ for different energy distributions of the suprathermal electrons as deduced from RPC-IES measurements. The diamonds correspond to the value used by Feldman et al. (2015): $q = 2$ and $E_0 = 25$ eV.

4.4×10^{-28} m^2 s^{-1} at 2.12, 1.64 and 1.56 au, respectively, which is a factor 13–15 larger than the values derived from the observations for the two periods in May and larger by about 33 for the observations in March. Moreover, we measured a larger coefficient k when the comet was at 2.8 au than 1.6 au suggesting another source of variability of the efficiency of the emissions.

Clark et al. (2015) and Broiles et al. (2016) have shown a large variability of the energetic electron distribution in the cometary environment resulting from the variability of the acceleration processes on the energetic electrons. Therefore, the value of $g(T_e)$ could be not correct for the observations performed in 2015 March and May. Clark et al. (2015) derived a parametrization of the velocity distribution of the suprathermal electrons ($10 < E < 300$ eV) given by

$$f(V) = A_q \frac{n_{e,s}}{4\pi V_0^3} \exp(-V/V_0)^q. \quad (13)$$

Converted to energy distribution function, this equation is written as

$$\frac{\Phi(E)}{n_{e,s}} = A_q \frac{V_0}{2E_0} \left(\frac{E}{E_0}\right) \exp(-E/E_0)^{q/2}, \quad (14)$$

where V_0 is the thermal velocity of the suprathermal electron, q is a shape parameter describing the shape of the distribution ($q = 2$ for a Maxwellian distribution), A_q is a normalization factor and $E_0 = 1/2 m_e {V_0}^2$, m_e being the electron mass. To estimate the possible variability of $g(T_e)$, we compute it from equations (12) and (13), and the cross-section displayed in Fig. 8 using different values of q and V_0 in the range given by Clark et al. (2015). Recently, Broiles et al. (2016) used a Kappa function to describe the warm electron population (energetic electrons most likely from cometary origin), differing from the distribution used by Clark et al. (2015). The change of distribution should not change the results presented in this paper.

We compute the variations of $g(T_e)$ from equation (12), using the energy distribution given by equation (14) and the cross-section displayed in Fig. 7. As shown in Fig. 8, the $g(T_e)$ function can vary by one order of magnitude for a given value of T_e, so we can expect a large variability of the efficiency of the water vapour dissociation by electron impact. A $g(T_e)$ value $\sim 8 \times 10^{-12}$ cm^3 s^{-1} could reconcile the observations presented here and the theoretical approach for case 1 presented in Section 3 for the observations in May but this value is in the lower range expected from the warm electron population observed by RPC-IES. Alternatively, a smaller α value (the fraction of suprathermal electrons) during the 2015 March and May observations compared to observations in 2014 December could also explain the differences but here again, the value used seems already low compared for example with the ratio derived by Madanian et al. (2016) at 20 km. Therefore, it seems difficult to reconcile the observations and the theory for the case 1: Assuming a suprathermal electron population proportional to the thermal electron population.

Alternatively, for a uniform warm population density (case 2), the excitation frequency is the product of the $g(T_e)$ function and the suprathermal electron density n_{es0}. For $g = 8 \times 10^{-11}$ cm^{-3}, we derive a suprathermal electron density of 52, 8, 28 and 20 cm^{-3} (Table 2). The first value is larger than the reported value by Madanian et al. (2016) in February 2015 and those derived by Broiles et al. (2016) in 2014 October 30. The other values are in the expected range. A $g(T_e)$ value increased by 2.5 ($T_e \sim 25$ eV) in 2014 December, closer to the value used by Feldman et al. (2015) would lead to density closer to the observations, suggesting a more efficient electron dissociative excitation of water vapour by suprathermal electron impact at this time. The range of T_e, n in this case seems more consistent with the RPC-IES measurements suggesting that the suprathermal electron density should be radially uniform, at few tens of kilometres above the nucleus in agreement with Madanian et al. (2016).

Though the observations done in March should be considered carefully because of the low signal-to-noise ratio, the efficiency of the mechanism derived from Alice and VIRTIS observations between 2014 December and 2015 May does not increase as expected from equation (10a) but instead seems to decrease from 2014 December to 2015 May. This suggests that the expected increase of the efficiency due to the increase of the ionization frequency ν is partly balanced by a decrease of $g(T_e)$ (or α for the case 1). The observations performed by RPC-IES indicate a decrease of the energetic electron temperature when the comet moves closer to the Sun (Broiles et al. 2016) which could explain the decrease of the efficiency of the electron dissociative excitation.

6 CONCLUSION

The UV emissions observed by Alice before the 67P/CG perihelion are mainly produced by water vapour dissociation by suprathermal electron impact, in which O and H atoms are produced in excited states and de-excite spontaneously. We used a simple theoretical approach to model this process and found the relation between the UV brightness and the water column density. We checked this simple model by using Lyman β Alice observations and VIRTIS observations of the water column density in 2014 December, 2015 March

and May. The electron dissociative excitation was more efficient in 2014 December compared to 2015 March and May. When we assume radial variations of the suprathermal electron density similar to the thermal electron population in $1/r$, the UV brightness should be proportional to the square of the water column density. For the observations in 2014 December, the relation is fulfilled within a factor 2–3, but it is difficult to reconcile this relation with the observations by RPC-IES for 2015 March and May observations. When we assume no radial variations of the suprathermal electron density, the UV brightness is proportional to the water column density and consistent with the observations by RPC-IES. A more careful comparison with the RPC-IES observations is deferred to a future study. The variability of the efficiency of the electron impact dissociation between the four other periods is not directly driven by the Sun–comet distance but is most likely associated with the variability of the suprathermal electron distribution.

ACKNOWLEDGEMENTS

Rosetta is an ESA mission with contributions from its member states and NASA. We thank CNES for sponsoring the French participations to Alice hardware and VIRTIS_H development, operations and scientific analysis. The Alice team acknowledges continuing support from NASA's Jet Propulsion Laboratory through contract 1336850 to the Southwest Research Institute. We thank an anonymous reviewer for the valuable comments and suggestions that has improved the manuscript.

REFERENCES

Bieler A. et al., 2015, A&A, 583, A7
Bockelée-Morvan D., Crovisier J., 1987, A&A, 187, 425
Bockelée-Morvan D., Crovisier J., Mumma M. J., Weaver H. A., 2004, in Comets II, Vol. 745. University of Arizona Press, Tucson, p. 391
Bockelée-Morvan D. et al., 2015, A&A, 583, A6
Broiles T. W. et al., 2016, J. Geophys. Res., 121, 7407
Clark G. et al., 2015, A&A, 583, A24
Coates A. J., 2004, Adv. Space Res., 33, 1977
Coradini A. et al., 2007, Space Sci. Rev., 128, 529
Crovisier J., 1987, A&A, 68, 223
Edberg N. J. T. et al., 2015, Geophys. Res. Lett., 42, 4263
Feldman P. D., Weaver H. A., Burgh E. B., 2002, ApJ, 576, 91
Feldman P. D. et al., 2015, A&A, 583, A8
Feldman P. D. et al., 2016, ApJ, 825, L8
Fink U. et al., 2016, Icarus, 277, 78
Fougere N., Altwegg K., Berthelier J.-J., Bieler A., Bockelée-Morvan D. et al., 2016a, MNRAS, 462, S156
Fougere N., Altwegg K., Berthelier J.-J., Bieler A., Bockelée-Morvan D. et al., 2016b, A&A, 588, A134
Galand M. et al., 2016, MNRAS, 462, S331
Hassig M. et al., 2015, Science, 347, 6220
Huebner W. F., Keady J. J., Lyon S. P., 1992, Astrophys. Space Sci., 195, 1
Itikawa Y., Mason N. 2005, J. Phys. Chem. Ref. Data, 34, 1
Körösmezey A. et al., 1987, J. Geophys. Res., 92, 7331
Le Roy L. et al., 2015, A&A, 583, A1
Lee S. et al., 2015, A&A, 583, A5
Lupu R. E., Feldman P. D., Weaver H. A., Tozzi G.-P., 2007, ApJ, 670, 1473
Luspay-Kuti A. et al., 2015, A&A, 583, A4
Madanian H. et al., 2016, J. Geophys. Res., 121, 5815
Makarov O. P., Ajello J. M., Vattipalle P., Kanik, I., Festou, M. C., Bhardwaj, A., 2004, J. Geophys. Res., 109, A09303
Migliorini A. et al., 2016, A&A, 589, 45
Nilsson H. et al., 2015, A&A 583, A20
Noonan J. et al., 2016, Acta Astronaut., 125, 3
Nordheim T. A., Jones G. H., Halekas J. S., Roussos E., Coates A. J., 2015, Planet. Space Sci., 119, 24
Odelstad E. et al., 2015. Res. Lett., 42, 126
Schunk R. W., Nagy A. F., (2009) Ionospheres: Physics, Plasma Physics, and Chemistry. Cambridge Univ. Press, Cambridge
Stern S. A. et al., 2007, Space Sci. Rev., 128, 507
Szego K. et al., 2000, Space Sci. Rev., 94, 429
Villanueva G. I., Mumma M. J., Boney B. P., Novak R. E., Barber R. J., DiSanti M. A., 2012, J. Quant. Spectrosc. Radiat. Transfer, 113, 202
Weaver H. A., Feldman P. D., Combi M. R., Krasnopolsky V., Lisse C. M., Shemansky D. E., 2002, ApJ, 576, L95
Weaver H. A., Feldman P. D., A'Hearn M. F., Dello Russo N., Stern S. A., 2011, ApJ, 734, L5
Zwinckl R. D., Baker D. N., Bame S. J., Feldman W. C., Fuselier S. A., Huebner, W. F., McComas, D. J., Young, D. T., 1986, Geophys. Res. Lett., 13, 401

This paper has been typeset from a Microsoft Word file prepared by the author.